Organic Electronics 88 (2021) 105996

Contents lists available at ScienceDirect

Organic Electronics

journal homepage: http://www.elsevier.com/locate/orgel

Benzodithiophene-based wide-bandgap small-molecule donors for organic photovoltaics with large open-circuit voltages

Eunhee Lee [a], Duyen K. Tran [b], Jihun Park [a], Wonyoung Ko [a], Samson A. Jenekhe [b,**], Ye-Jin Hwang [a,*]

[a] Department of Chemistry and Chemical Engineering, Education and Research Center for Smart Energy and Materials, Inha University, 100 Inha-ro, Michugol-gu, Incheon, Republic of Korea

[b] Department of Chemical Engineering and Department of Chemistry, University of Washington, Seattle, WA, 98195-1750, United States

ARTICLE INFO

Keywords:
Benzodithiophene
Fluorination
Alkylthiolation
Small-molecule donor
Organic photovoltaics

ABSTRACT

We have developed new small-molecule electron donors, SMBDT-S and SMBDT-SF, based on benzo[1,2-*b*:4,5-*b*']dithiophene (BDT) with thiophene side chains as a core unit and rhodanine end-capping units to enhance the open-circuit voltage (V_{oc}), which is one of the factors limiting performance of small-molecule organic photovoltaics (OPVs). The SMBDT-S and SMBDT-SF donor molecules exhibited excellent thermal stability and high crystallinity. SMBDT-S was found to have a wide bandgap of 1.85 eV with the highest occupied molecular orbital (HOMO) energy level of − 5.56 eV. The fluorination in SMBDT-SF led to the same bandgap of 1.86 eV with an even lower-lying HOMO energy level of − 5.72 eV. Both SMBDT-S and SMBDT-SF have large thin-film absorption coefficients of (1.4–1.5) × 10^5 cm^{-1}. Bulk heterojunction OPV devices based on pairing SMBDT-S and SMBDT-SF respectively with $PC_{71}BM$ electron acceptor showed V_{oc} as high as 1.18 eV, which is among the highest V_{oc} reported for all-small-molecule solar cells. These results demonstrate that introducing fluorine atoms and alkylthio side chains are effective strategies to downshift the HOMO energy level and enhance the V_{oc} in OPVs.

1. Introduction

Most of the high performing organic photovoltaics (OPVs) are based on polymer donors, and the maximum power conversion efficiency (PCEs) of polymer based OPVs has recently reached up to 17% [1–4]. The use of polymer donors in OPVs, however, has significant performance reproducibility issues due to the batch-to-batch variations of morphological properties, which are mainly determined by the molecular weight and molecular weight dispersity (*Đ*) [5–10]. Small-molecule (SM) donors have recently attracted much attention as potential replacements for polymer donors since they can overcome batch-to-batch variation issues with their well-defined chemical structures [5,6,10–22]. So far, the criteria used in the design of SM donor materials include a broad absorption spectrum, sufficient material crystallinity for high charge carrier mobility, and matching energy levels and energy offsets with acceptors for high open-circuit voltage (V_{oc}) and efficient charge separation. Based on these design criteria, a number of new SM donors have been developed and the maximum PCE of OPVs based on SM donors has reached over 14% [15,23–25]. Since the performance of SM based OPVs is still inferior to that of polymer donor based OPVs, studies are needed on the design criteria that can improve the open-circuit voltage (V_{oc}), one of the limiting photovoltaic parameter in the SM based OPVs [26–30].

A key requirement to achieve high V_{oc} is to maintain a low-lying highest occupied molecular orbital (HOMO) energy level while ensuring sufficient energetic offset between donor and acceptor molecules for efficient exciton dissociation. Various molecular engineering strategies have been reported to lower the HOMO energy levels of SM donors, including the introduction of alkyl [26,31–34], alkylthio [26,35–43], or alkoxy [26,40,44,45], side chains, and halogen atoms [26,35–39,46–52]. Among these methods, introducing alkylthio side chains and halogen atoms are known to be among the most effective strategies to significantly tune HOMO energy levels (~0.2 eV). In the case of alkylthiolation, sulfur atoms withdraw the π-electrons from the main

* Corresponding author
** Corresponding author
E-mail addresses: jenekhe@u.washington.edu (S.A. Jenekhe), yjhwang@inha.ac.kr (Y.-J. Hwang).

https://doi.org/10.1016/j.orgel.2020.105996
Received 16 September 2020; Received in revised form 18 October 2020; Accepted 19 October 2020
Available online 4 November 2020

backbone, and thus lowers the HOMO energy level [26,42]. The introduction of halogen atoms, specifically fluorine atoms, can lead to a simultaneous downshift of both the HOMO and LUMO energy levels without compromising the molecular conformations due to the strong electron-withdrawing effects induced by the small fluorine atoms.

In this paper, we report the development of two new small-molecule donors, SMBDT-S and SMBDT-SF, based on the core benzo[1,2-*b*:4,5-*b'*] dithiophene (BDT) moiety with thiophene side chains towards the study of effects of alkylthiolation and fluorination on donor material properties and V_{oc}. SMBDT-S is designed to have alkylthio side chains and SMBDT-SF has alkylthio side chains and fluorine atoms on the thiophene side chains (Fig. 1). The thermal and optical properties, and electronic structures of the donor molecules were investigated. Both SMBDT-S and SMBDT-SF molecules were found to have excellent thermal stability featuring high decomposition temperature (T_d) above 300 °C. SMBDT-S has a wide electrochemical energy bandgap (E_g^{el}) of 2.00 eV with the HOMO energy level of − 5.56 eV whereas SMBDT-SF has a wider E_g^{el} of 2.13 eV with lower HOMO energy level of − 5.72 eV as a result of fluorination. Broad optical absorption bands in the range of 300–700 nm were observed with an absorption coefficient (α) on the order of 10^5 cm^{-1} in both small molecules. The photovoltaic properties of the donor molecules were characterized by fabricating OPVs using their respective binary blends with fullerene ($PC_{71}BM$) as an electron acceptor. The SMBDT-S:$PC_{71}BM$ blend devices gave the highest performance (*PCE* = 2.9%, J_{sc} = 5.6 mA/cm^2, V_{oc} = 1.05 V, *FF* = 0.5) in conventional device architecture with solvent vapor annealing. Under the same processing conditions, the SMBDT-SF:$PC_{71}BM$ blend devices gave an enhanced V_{oc} of 1.18 V, which is the highest V_{oc} reported for SM based OPVs. However, very limited short-circuit current of 1.40 mA/cm^2 was observed, and thus a much lower *PCE* of 0.9% was obtained. These results showed that the alkylthiolation and fluorination are effective strategies to achieve high V_{oc}, although further studies using different acceptors and modifying the chemical structures of the donor molecules to fine-tune their solubility and in turn the bulk morphology are needed to achieve higher performance in OPVs.

2. Experimental

2.1. Materials

Benzo[1,2-*b*:4,5-*b'*]dithiophene-4,8-dione, *N*-fluorobenzenesulfonimide, 3-ethylrhodanine were purchased from TCI. All other chemicals were purchased from Sigma-Aldrich and used as received. (4,8-bis(5-((2-ethylhexyl)thio)-4-fluorothiophen-2-yl)benzo[1,2-*b*:4,5-*b'*]dithiophene-2,6-diyl)bis (trimethylstannane) (BDT-S) and (4,8-bis(5-((2-ethylhexyl)thio)thiophen-2-yl)-4,8-dihydrobenzo [1,2-*b*:4,5-*b'*]dithiophene-2,6-diyl)bis(trimethylstannane) (BDT-SF) were synthesized according to the known literature procedures [35,38].

5,5'-(4,8-bis(5-((2-ethylhexyl)thio)thiophen-2-yl)benzo[1,2-*b*:4,5-*b'*]dithiophene-2,6-diyl)bis(3-octylthiophene-2-carbaldehyde)

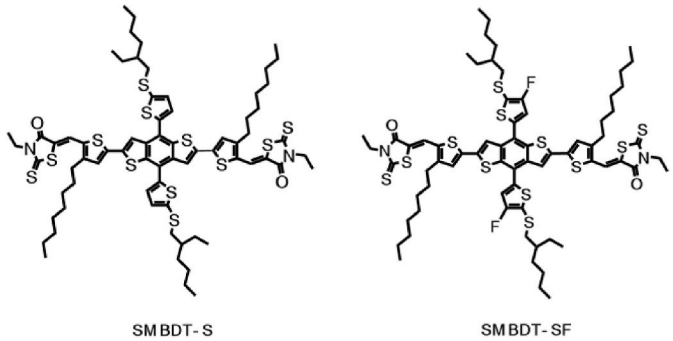

Fig. 1. Molecular structures of SMBDT-S (a) and SMBDT-SF (b).

(Compound 2). BDT-S (0.358 mmol, 0.357 g), compound **1** (1.00 mmol, 0.3 g) and $Pd(PPh_3)_4$ (0.018 mmol 21.3 mg) were dissolved in 30 mL of anhydrous toluene under nitrogen atmosphere. The reaction was carried out at 100 °C for 48 h. After the reaction was cooled to room temperature, the reaction mixture was quenched by adding deionized water, and extracted with dichloromethane. The organic phase was dried over anhydrous magnesium sulfate. Compound **2** was obtained by column chromatography (eluent: hexane/dichloromethane) as a reddish orange solid (0.118 g, Yield = 30%). ^{1}H NMR ($CDCl_3$, 400 MHz): δ (ppm) 9.87 (s, 2H), 7.78 (s, 2H), 7.64 (s, 2H), 7.38 (s, 2H), 7.26 (s, 2H), 2.98 (d, 4H), 2.89 (t, 4H), 1.69 (m, 6H), 1.53–1.27 (br, 36H), 0.91 (m, 18H).

(5*Z*,5′*Z*)-5,5'-((5,5'-(4,8-bis(5-((2-ethylhexyl)thio)thiophen-2-yl)benzo [1,2-*b*:4,5-*b'*] dithiophene-2,6-diyl)bis(3-octylthiophene-5,2-diyl))bis(methanylylidene))bis(3-ethyl-2-thioxothiazolidin-4-one) (SMBDT-S). Compound **2** (0.108 mmol, 0.118 g), 3-ethylrhodanine (0.17 mmol, 0.17 g) were dissolved in 30 mL of anhydrous chloroform under nitrogen atmosphere and 0.2 mL of piperidine was added. The reaction mixture was refluxed for 24 h. After the reaction was cooled to room temperature, the organic phase was extracted with chloroform and dried over anhydrous magnesium sulfate. SMBDT-S was obtained by column chromatography (eluent: hexane/chloroform) as a dark purple solid (96 mg, Yield = 54%). ^{1}H NMR ($CDCl_3$, 400 MHz): δ (ppm) 7.81 (s, 2H), 7.74 (s, 2H), 7.41 (s, 2H), 7.25 (s, 4H), 4.22 (d, 4H), 3.01 (d, 4H), 2.87 (t, 4H), 1.69 (m, 6H), 1.53–1.27 (br, 36H), 0.94 (m, 18H).

5,5'-(4,8-bis(5-((2-ethylhexyl)thio)-4-fluorothiophen-2-yl)benzo [1,2-*b*:4,5-*b'*]dithiophene-2,6-diyl)bis (3-octylthiophene-2-carbaldehyde) (Compound 3). BDT-SF (0.955 mmol, 0.96 g), compound **1** (2.62 mmol, 0.79 g) and $Pd(PPh_3)_4$ (0.047 mmol 55.2 mg) were dissolved in 100 mL of anhydrous toluene under nitrogen atmosphere. The reaction was carried out 100 °C for 48 h. After the reaction was cooled to room temperature, quenched by adding deionized water, and extracted with dichloromethane. The organic phase was dried over anhydrous magnesium sulfate. Compound **3** was obtained by column chromatography (eluent: hexane/dichloromethane) as a reddish orange solid (0.61 g, Yield = 58%).^{1}H NMR ($CDCl_3$, 400 MHz): δ (ppm) 9.89 (s, 2H), 7.77 (s, 2H), 7.65 (s, 2H), 7.25 (s, 2H), 2.94 (d, 4H), 2.88 (t, 4H), 1.68 (m, 6H), 1.52–1.32 (br, 36H), 0.91 (m, 18H).

(5*Z*,5′*Z*)-5,5'-((5,5'-(4,8-bis(5-((2-ethylhexyl)thio)-4-fluorothiophen-2-yl)benzo [1,2-*b*:4,5-*b'*] dithiophene-2,6-diyl)bis(3-octylthiophene-5,2-diyl))bis(methanylylidene))bis(3-ethyl-2-thioxothiazolidin-4-one) (SMBDT-SF). Compound **3** (0.39 mmol, 0.434 g), 3-ethylrhodanine (3.9 mmol, 0.63 g) were dissolved in 60 mL of anhydrous chloroform under nitrogen atmosphere and 0.4 mL of piperidine was added. The reaction mixture was refluxed for 24 h. After the reaction was cooled to room temperature, the organic phase was extracted with chloroform and dried over anhydrous magnesium sulfate. SMBDT-SF was obtained by column chromatography (eluent: hexane/chloroform) as a dark purple solid (0.3 g, Yield = 54%). ^{1}H NMR ($CDCl_3$, 400 MHz): δ (ppm) 7.81 (s, 2H), 7.71 (s, 2H), 7.25 (s, 4H), 4.22 (d, 4H), 2.94 (d, 4H), 2.88 (t, 4H), 1.69 (m, 6H), 1.50–1.27 (br, 36H), 0.96 (m, 18H).

2.2. Characterization

The chemical structures of all compounds were confirmed by ^{1}H NMR, and ^{1}H NMR spectra at 400 MHz were recorded on a Bruker Avance III spectrometer. Thermal properties of SMBDT-S and SMBDT-SF were measured by thermogravimetric analysis (TGA) and differential scanning calorimetry (DSC). TGA thermograms were acquired on a NETZSCH TG209F3 at a heating rate of 20 °C per minutes up to 550 °C under nitrogen gas flow. DSC thermograms were obtained from a PerkinElmer Jade DSC Lab system under nitrogen gas flow at a heating and cooling rate of 20 °C per minutes up to 310 °C for SMBDT-S and 20 °C per minutes up to 280 °C for SMBDT-SF.

The optical properties were investigated by PerkinElmer Lambda 25 UV/VIS spectrometer, and the photoluminescence (PL) emission spectra

were obtained with a Photon Technology International (PTI) Inc. model QM2001-4 spectrofluorimeter (excitation wavelength = 565 nm). The absorption spectra of solution and solid-state were obtained from diluted (10^{-6} M) small molecule solutions in chloroform and as thin films on glass substrates, respectively. Cyclic voltammograms were obtained by Digi-Ivy DY2300 Series Potentiostat in an electrolyte solution of 0.1 M tetrabutylammonium hexafluorophosphate (Bu_4NPF_6) in acetonitrile at a scan rate of 50 mV/s, and the electrolyte solution was deoxygenated using nitrogen bubbling for 15 min before use. Ag/Ag^+ (Ag in 0.1 M $AgNO_3$ solution) was used as a reference electrode, and platinum wires were used as working and counter electrodes. Ferrocene/ferrocenium (Fc/Fc^+) was used as an internal standard. The samples for CV were prepared by dip-coating the concentrated small molecule solutions in chloroform onto Pt wires.

X-ray diffraction (XRD) was performed on a Bruker-AXS New D8-Advance with a Cu-Kα beam by using films drop-casted glass substrates from concentrated solutions in chloroform, followed by annealing at 200 °C for 10 min.

The geometrically optimized structures, electronic energy levels, and optical absorption profile of new small molecule donors were calculated based on density functional theory (DFT) and time-dependent (TD) DFT with the B3LYP functional and the 6-31G(d) basis set using the Firefly 8.2.0 software package.

2.3. Fabrication and characterization of organic photovoltaic devices

Solar cell devices were fabricated with a conventional architecture of ITO/PEDOT:PSS/Blend/PFN-Br/Al. ITO-coated substrates (15 Ω/square, Shanghai B. Tree Tech, Shanghai, China) were cleaned sequentially in ultrasonic baths with detergent, deionized water, acetone, and isopropyl alcohol for 30 min, dried using nitrogen gas, and followed by 10 min of O_2 plasma cleaning. The PEDOT:PSS (Clevios Al 4083) dispersion was filtered and spin-coated onto the ITO substrates and followed by thermal annealing at 150 °C for 10 min to make ~ 40 nm thick PEDOT:PSS layer. The SMBDT-S:$PC_{71}BM$ (1:0.5) blends were prepared in chloroform, mixed and stirred overnight at 60 °C in an Argon-filled glovebox. The SMBDT-SF:$PC_{71}BM$ (1:0.5) blends were prepared in the same manner. The blend solutions were spin-coated at 1000 rpm for 50 s in the Argon-filled glovebox. The samples underwent solvent vapor annealing procedure by exposing to a chloroform-filled Petri dish for 60 s. All the active layers had a thickness of 100±3 nm. PFN-Br was dissolved in methanol (0.5 mg/mL) and spin-coated onto the active layer at 2000 rpm for 40 s. The samples were then transferred to an evaporation chamber where aluminum (100 nm) was thermally deposited. An aperture mask with area of 3.14 mm^2 is applied during measurements to define the illuminated device area. After evaporation of the electrode, the photovoltaic cells were tested under AM 1.5G solar illumination at 100 mW/cm^2 in ambient air by using a solar simulator (Model 16S, Solar Light Co., Philadelphia, PA) with a 200W Xenon Lamp Power Supply (Model XPS 200, Solar Light Co., Philadelphia, PA) calibrated by NREL certified Si photodiode (Model 1787–04, Hamamatsu Photonics K·K., Japan) and a HP4155A semiconductor parameter analyzer (Yokogawa Hewlett Packard, Japan). After the *J-V* measurement, the external quantum efficiency (EQE) was measured by using a solar cell quantum efficiency measurement system (Model QEX10, PV Measurements, Inc., Boulder, CO) with a 2 mm^2 (2 mm × 1 mm) size masked incident light source and TF Mini Super measurement apparatus for multiple devices in a single substrate. The EQE system was calibrated with a Si photodiode before measurement. AFM characterization of surface morphology was done on the active layers of the actual BHJ solar cells by using a Veeco Dimension 3100 scanning probe microscope (SPM) system.

3. Results and discussions

3.1. Material synthesis

The two small-molecule donors, SMBDT-S and SMBDT-SF, were designed based on the BDT unit with thiophene side chains, 4,8-bis(5-((2-ethylhexyl)thio)thiophen-2-yl)benzo[1,2-*b*:4,5-*b'*]dithiophene (BDT-S) and 8-bis(5-((2-ethylhexyl)thio)-4-fluorothiophen-2-yl)benzo[1,2-*b*:4,5-*b'*]dithiophene (BDT-SF), respectively, as a core unit. BDT-S includes thiolated alkyl chains and BDT-SF includes both thiolated alkyl chains and fluorine atoms on the thiophene side chains. On both sides of the BDT monomer is a 3-octylthiophene spacer (Fig. 1). Both small-molecules are end-capped with 3-ethylrhodanine, resulting in the realization of a donor-acceptor intramolecular charge transfer effect [53–55].

BDT-S and BDT-SF were synthesized according to the known literature procedures [35,38,56], and detailed synthetic procedures are provided in the Supporting Information. Stille coupling reactions of BDT-S and BDT-SF with compound **1** in the presence of $Pd(PPh_3)_4$ gave the aldehyde intermediates, and the target small-molecule donors were obtained by Knoevenagel reaction (Scheme 1). We note that the yield of the Stille coupling reaction to synthesize compound **2** was low (30%) because of the low purity of BDT-S (32.6%), which was obtained as a liquid and thus could not be purified by recrystallization; the purity of BDT-S was determined via the ^1H NMR spectrum (Fig. S1). The final Knoevenagel reaction gave 54% yield for both SMBDT-S and SMBDT-SF, and these yields are comparable to the reported values of similar condensation reactions [57]. After purification by column chromatography with hexane and chloroform mixed solvent as an eluent, SMBDT-S and SMBDT-SF were obtained as dark purple solids. The molecular structure of the monomers and final products, SMBDT-SF and SMBDT-S, were confirmed by ^1H NMR spectroscopy (Figs. S1–S16).

Thermogravimetric analysis (TGA) and differential scanning calorimetry (DSC) scans of SMBDT-S and SMBDT-SF showed that they exhibit good thermal stability with a decomposition temperature (T_d) of 333 °C and 348 °C, respectively, at 5% weight loss (Fig. S17). The melting temperatures (T_m) for SMBDT-S and SMBDT-SF was observed at 285.2 °C and 269.6 °C, respectively, and the crystallization temperatures (T_c) were observed at 269.6 °C and 222 °C, respectively (Fig. S18). The melting and crystallization enthalpies calculated as the area of the endothermic and exothermic DSC peaks, respectively, were higher in SMBDT-SF than in SMBDT-S. In addition, the larger difference between T_m and T_c in SMBDT-SF (47.6 °C) than in SMBDT-S (15.6 °C) suggests that SMBDT-SF has higher crystallinity than SMBDT-S. SMBDT-SF and SMBDT-S, both were soluble in chloroform (15 mg/mL), whereas they had limited solubility in other common organic solvents (THF, dichloromethane, chlorobenzene). Solubility of this class of donor materials could be improved by using the longer and branched alkyl side chains or through the alkyl chains on the end rhodanine units.

3.2. Optical and electrochemical properties

The UV–Vis absorption spectra of SMBDT-S and SMBDT-SF in both solution and thin-film are shown in Fig. 2 and the corresponding numerical optical properties are summarized in Table 1. In dilute chloroform solution (10^{-6} M), SMBDT-S and SMBDT-SF showed two absorption bands in the range of 300–400 nm and 400–600 nm, which correspond respectively to the π–π* transition and the intramolecular charge transfer (ICT) interaction between the BDT and the rhodanine units [53–55]. The thin-film absorption spectra of both SMBDT-S and SMBDT-SF are significantly red-shifted by about 50 nm relative to the solution spectra (Fig. 2) because of the enhanced π-π intermolecular interactions and conformational changes in the solid state [47,58]. As expected, SMBDT-SF showed a 35% higher maximum extinction coefficient (ε) of $6.46 \times 10^4\ M^{-1}\ cm^{-1}$ compared to that of SMBDT-S because fluorination is known to enhance the extinction coefficient [35,47]. The

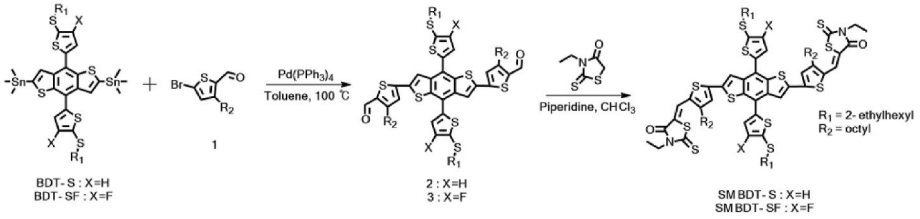

Scheme 1. Synthetic route to SMBDT-S and SMBDT-SF.

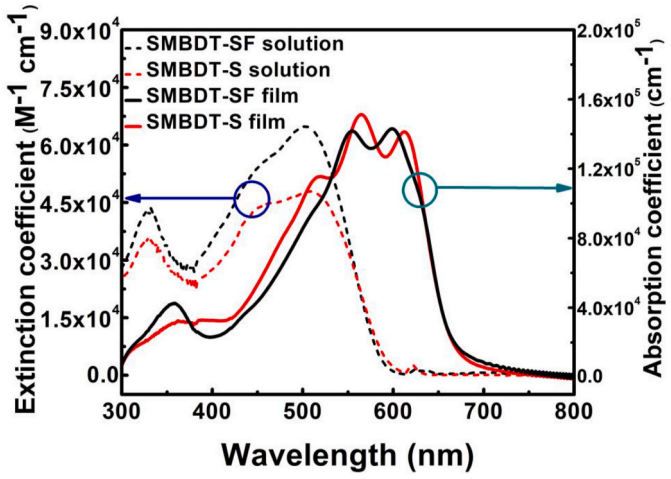

Fig. 2. UV–Vis absorption spectra of SMBDT-S (red) and SMBDT-SF (black) in solutions (dotted line) and as thin films on glass substrates (solid line). (For interpretation of the references to colour in this figure legend, the reader is referred to the Web version of this article.)

thin-film absorption coefficients of both small molecules were found to be 1.51 x 10^5 cm^{-1} (at 565 nm) and 1.43 x 10^5 cm^{-1} (at 599 nm) for SMBDT-S and SMBDT-SF, respectively, which are an order of magnitude higher compared to the reported α for similar small-molecule donors [59–63]. The observed higher absorption coefficient can be rationalized by the increased packing density as a result of a highly planar backbone as evidenced by the density functional theory (DFT) calculated molecular structures (Fig. S19). SMBDT-S already has large crystallites and tends to have a face-on orientation according to DFT calculation and XRD analysis, and thus no significant fluorination effect was observed on the absorption coefficient of SMBDT-SF. The superior absorption coefficient in these new donor molecules suggest efficient photon harvesting which is highly beneficial for OPV applications. The optical band gap (E_g^{opt}), determined from the onset absorption band edge, is identical 1.85–1.86 eV for SMBDT-S and SMBDT-SF. The observed identical E_g^{opt} values for SMBDT-S and SMBDT-SF is consistent with the result from DFT calculation (Fig. S19).

The electronic structures of SMBDT-S and SMBDT-SF were measured by cyclic voltammetry (CV) and are summarized in Table 1 whereas the cyclic voltammograms are shown in Fig. 3. The highest occupied molecular orbital (HOMO)/the lowest unoccupied molecular orbital (LUMO) energy levels were − 5.56/− 3.56 eV for SMBDT-S and − 5.72/− 3.59 eV for SMBDT-SF, as calculated from the CV onset redox potentials. The presence of highly electronegative fluorine atoms on SMBDT-SF led to lower-lying HOMO/LUMO energy levels compared to those of SMBDT-S, which is in good agreement with other reports on the effects of fluorination [64,65]. Moreover, the HOMO energy level (− 5.72 eV) of SMBDT-SF is lower-lying than most of the HOMO energy levels reported for small-molecule donors and this is a result of the synergistic effect of fluorination and alkylthio side chains [11,12,14,35,38,39]. Compared to the LUMO energy levels of many fullerene and non-fullerene acceptors, the LUMO energy levels of these new small-molecule donors can give sufficient energy offsets for efficient charge separation [66]. Similarly, the deep HOMO levels of SMBDT-S and SMBDT-SF suggest that a large V_{oc} can be expected in OPV devices fabricated from them.

3.3. Morphological properties

The molecular packing structure and bulk crystallinity of the new small molecules were characterized by X-ray diffraction analysis (XRD) of thermally annealed (200 °C, 10 min) drop-casted films. As shown in Fig. 4, XRD patterns of both SMBDT-S and SMBDT-SF showed an intense lamellar (100) peak at 2θof 4.27° and 2θof 4.32°, respectively, and no other peaks were observed. The calculated *d*-spacing from this lamellar peak was 20.65 Å for SMBDT-S and 20.44 Å for SMBDT-SF, and this similar *d*-spacing in the two small-molecule donors means that the fluorination had no impact on the backbone packing. Moreover, these *d*-spacing is shorter than the length of side chains on SMBDT-S and SMBDT-SF, which suggests inter-digitation of the side chains [69]. Although both materials gave similar *d*-spacing values, SMBDT-SF showed slightly narrower (100) diffraction peak with the full width at half maximum (FWHM) of 0.1499° compared to the FWHM of 0.1928° in SMBDT-S. This result suggests that SMBDT-SF had a higher crystallinity than SMBDT-S which can be explained by the enhanced intermolecular interactions from the noncovalent F···H and F···S interactions facilitated by the fluorine atoms [47]. This result is in good agreement with the DSC results discussed above.

3.4. Photovoltaic properties

We characterized the photovoltaic properties of the new small-molecule donors by fabricating bulk heterojunction OPV devices using $PC_{71}BM$ as the electron acceptor. The optimal device fabrication conditions were found by varying the donor/acceptor (D/A) blend ratio, the device architecture, the use of solvent processing additives, and the post-deposition conditions (thermal annealing/solvent vapor annealing) of the active layer. First, the SMBDT-S:$PC_{71}BM$ devices with different D/A

Table 1
Optical properties and electronic structures of SMBDT-S and SMBDT-SF donor molecules.

small-molecule	λ_{max}^{sol} [nm]	λ_{max}^{film} [nm]	α_{max} [M^{-1} cm^{-1}]	E_g^{opt} [eV]	LUMO [eV] [a]	HOMO [eV] [b]	E_g^{el} [eV]
SMBDT-S	509	565	1.51×10^5	1.85	−3.56	−5.56	2.00
SMBDT-SF	504	599	1.43×10^5	1.86	−3.59	−5.72	2.13

[a] LUMO energy was calculated based on LUMO = − (q (E_{red} − $E^{Fc/Fc+}$) + 4.8 eV).
[b] HOMO energy was calculated based on HOMO = − (q (E_{oxi} − $E^{Fc/Fc+}$) + 4.8 eV [67,68].

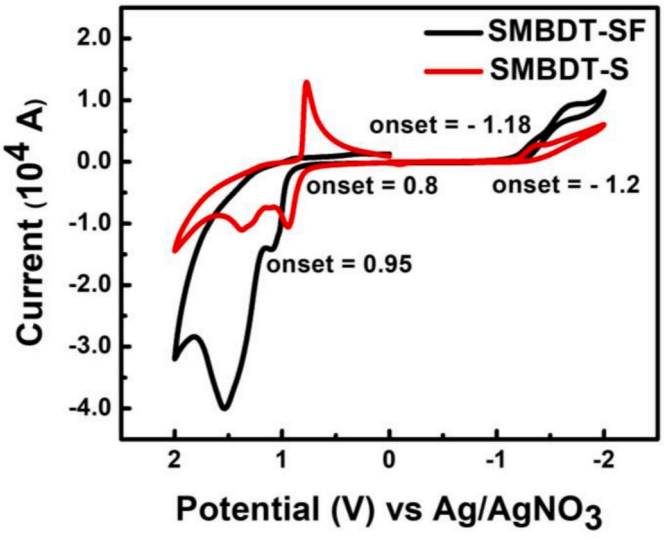

Fig. 3. Cyclic Voltammograms of SMBDT-S and SMBDT-SF in 0.1 M Bu_4NPF_6 solution in acetonitrile.

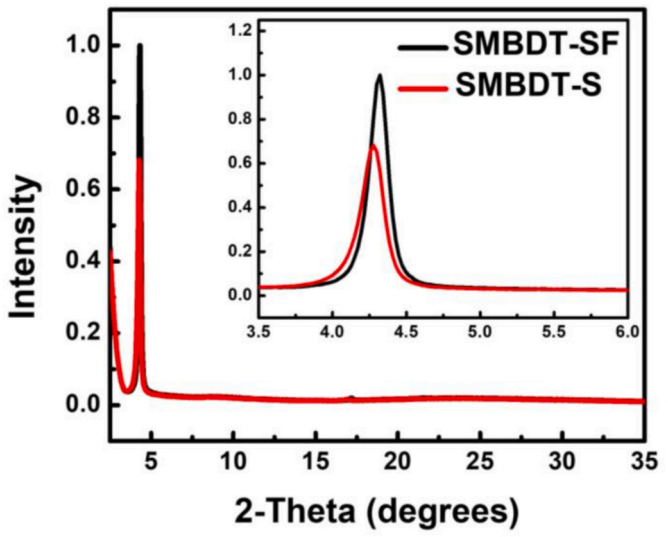

Fig. 4. XRD patterns of SMBDT-S (red) and SMBDT-SF (black) films annealed at 200 °C for 10 min. (For interpretation of the references to colour in this figure legend, the reader is referred to the Web version of this article.)

blend ratios (1:0.5, 1:0.8, 1:1, 1:1.5) in inverted structure of indium tin oxide (ITO)/ZnO/PEI/active layer/MoO_3/Ag were characterized, where polyethyleneimine (PEI) was used as a cathode interlayer [70]. The blend devices of lower donor compositions were found to have slightly enhanced photovoltaic parameters with the highest PCE of 1.22% achieved with a D/A blend ratio of 1:0.5 (Table S2). The photovoltaic properties of SMBDT-S:$PC_{71}BM$ devices were found to be improved by using a conventional device architecture of ITO/PEDOT:PSS/active layer/PFN-Br/Al where poly (3,4-ethylenedioxythiophene) polystyrene sulfonate (PEDOT:PSS) was the hole-transporting layer, and poly (9, 9-bis(3'-(*N,N*-dimethyl)-*N*-ethylammonium-propyl-2,7-fluorene)-alt-2, 7-(9,9-dioctylfluorene))dibromide (PFN–Br) was the electron-transporting layer. The SMBDT-S:$PC_{71}BM$ conventional devices processed by annealing at 110 °C for 10 min gave rise to an improved PCE of 2.41% with an enhanced J_{sc} of 5.04 mA/cm^2, a V_{oc} of 1.04 V, and a *FF* of 0.38. After solvent vapor annealing (SVA) with chloroform, the SMBDT-S:$PC_{71}BM$ devices had slightly enhanced photovoltaic parameters ($J_{sc} = 5.22$ mA/cm^2, $V_{oc} = 1.05$ V, $FF = 0.48$); thus, a maximum PCE of 2.9% was achieved. Further optimization by varying the SVA treatment time or using different solvent processing additives (Tables S3 and S4) led to minimal changes in the photovoltaic properties.

The SMBDT-SF: $PC_{71}BM$ devices were fabricated using the same processing conditions as the optimal SMBDT-S:$PC_{71}BM$ devices (Fig. 5 (a) and Table 2), however, they resulted in a maximum PCE of 0.9%. This is due to the extremely low photocurrent (1.4 mA/cm^2). This poor PCE seen in SMBDT-SF:$PC_{71}BM$ devices can be explained by poor bulk film morphology with largely aggregated phases and the modest solubility of SMBDT-SF molecules. Nevertheless, it is worth noting that the observed V_{oc} of 1.18 V is among the highest value reported so far for all-small-molecule fullerene-based OPVs [71]. Thus, the observed high V_{oc} (> 1V) observed in both SMBDT-S and SMBDT-SF devices suggests that the alkylthiolation and fluorination of small-molecule donors are the effective design strategies to achieve enhanced V_{oc}. The observed high V_{oc} in these SMBDT-S and SMBDT-SF based devices also suggested that they are promising candidates to be used in tandem OPVs to ultimately achieve a V_{oc} beyond 2V, which can be beneficial for water splitting applications [72,73]. We believe that better device performances can be realized in future studies by using compatible acceptors and further modification of the molecular structures of these donor molecules to improve solubility and overall bulk morphology. The external quantum efficiency (EQE) spectra of the best SMBDT-S:$PC_{71}BM$ and SMBDT-SF:$PC_{71}BM$ devices are shown in Fig. 5(b). Both devices exhibited broad photoresponses in range of 300–700 nm, and the peak EQE values were 33% at 550 nm in SMBDT-S devices and 5.5% at 540 nm in SMBDT-SF device. The observed EQE spectra matched well with the optical absorption spectra of SMBDT-S and SMBDT-SF. We further investigated morphological properties of two active layers, SMBDT-S:$PC_{71}BM$ blend and SMBDT-SF:$PC_{71}BM$ blend, by atomic force microscopy (AFM). As shown in Fig. S23 and Fig. S24, height and phase images of SMBDT-SF:$PC_{71}BM$ blend showed clear phase separations and aggregates with higher root mean square (RMS) roughness of 2.0 nm than in SMBDT-S:$PC_{71}BM$ blend (RMS value = 1.5 nm). This result indicates stronger phase separation behavior of SMBDT-SF than SMBDT-S, and can partially explain lower EQE values in SMBDT-SF:$PC_{71}BM$ devices compared to SMBDT-S:$PC_{71}BM$ devices.

3.5. Conclusions

We have designed and synthesized two new BDT-based small-molecule donors, SMBDT-S with alkylthio-groups and SMBDT-SF with alkylthio-groups and fluorine atoms, and investigated their thermal, optical, electronic structure, and photovoltaic properties. Both small-molecules were found to exhibit excellent thermal stability and broad absorption spectra spanning from 300 nm to 700 nm featuring high absorption coefficients of (1.4–1.5) × 10^5 cm^{-1}. The observed wide bandgaps (> 1.8 eV) with low-lying HOMO energy levels (< −5.5 eV) of SMBDT-S and SMBDT-SF suggest that they have good potential for developing efficient OPVs having large V_{oc} above 1.0 V. Initial characterization of their photovoltaic properties by using $PC_{71}BM$ as an electron acceptor produced SMBDT-S:$PC_{71}BM$ devices with a maximum PCE of 2.9% and a V_{oc} of 1.05 V whereas the SMBDT-SF:$PC_{71}BM$ devices gave a maximum PCE of 0.90% with a V_{oc} of 1.18 V. Although the observed power conversion efficiencies in this study were relatively low, we point out that the V_{oc} (1.18 eV) of the devices is the highest value reported for the small-molecule donor based OPVs. Indeed, the observed high V_{oc} (1.18 V) is among the highest value reported so far for all-small-molecule based OPVs. Improved photovoltaic device performance can be expected from this new class of small-molecule donors by improving the solubility of the small-molecules via longer alkyl side chains and by pairing them with more compatible acceptors.

Declaration of competing interest

The authors declare that they have no known competing financial

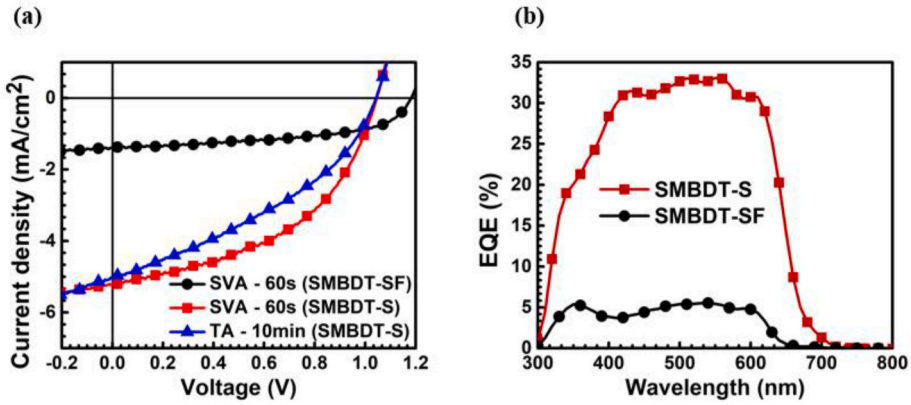

Fig. 5. (a) *J-V* curves of SMBDT-S:$PC_{71}BM$, SMBDT-SF:$PC_{71}BM$ devices after solvent vapor annealing (SVA) for 60 s, and SMBDT-S:$PC_{71}BM$ device after thermal annealing (TA) at 110 °C for 10 min. (b) EQE spectra of optimized SMBDT-S:$PC_{71}BM$ and SMBDT-SF:$PC_{71}BM$ devices in conventional architecture.

Table 2
Photovoltaic properties of the optimized SMBDT:$PC_{71}BM$ and SMBDT-SF:$PC_{71}BM$ blend devices.

Blend (1:0.5) [a]	J_{sc} (mA/cm^2)	V_{oc} (V)	FF	PCE (%)
SMBDT-SF:$PC_{71}BM$[b,d]	1.39 (1.44 ± 0.13)	1.18 (1.16 ± 0.02)	0.55 (0.44 ± 0.07)	0.90 (0.74 ± 0.13)
SMBDT-S:$PC_{71}BM$[b,d]	5.55 (4.86 ± 0.32)	1.05 (1.09 ± 0.03)	0.50 (0.49 ± 0.02)	2.89 (2.62 ± 0.17)
SMBDT-S:$PC_{71}BM$[c,e]	5.68 (5.04 ± 0.47)	1.04 (1.04 ± 0.01)	0.41 (0.38 ± 0.02)	2.41 (1.99 ± 0.29)

[a] Conventional device structure (ITO/PEDOT:PSS/Blend/PFN-Br/Al).
[b] Devices treated with 60 s of solvent vapor annealing.
[c] Devices treated by annealing at 110 °C for 10 min.
[d] The photovoltaic properties were averaged over 10 devices.
[e] The photovoltaic properties were averaged of 4 devices.

interests or personal relationships that could have appeared to influence the work reported in this paper.

Acknowledgements

Our work was supported by the NRF Korea, NRF-2018R1C1B5046181. Work at the University of Washington Seattle was supported by the National Science Foundation (CBET- 1803245).

Appendix A. Supplementary data

Supplementary data to this article can be found online at https://doi.org/10.1016/j.orgel.2020.105996.

References

[1] L. Meng, Y. Zhang, X. Wan, C. Li, X. Zhang, Y. Wang, X. Ke, Z. Xiao, L. Ding, R. Xia, Organic and solution-processed tandem solar cells with 17.3% efficiency, Science 361 (2018) 1094–1098.
[2] L. Zhan, S. Li, T.-K. Lau, Y. Cui, X. Lu, M. Shi, C.-Z. Li, H. Li, J. Hou, H. Chen, Over 17% efficiency ternary organic solar cells enabled by two non-fullerene acceptors working in an alloy-like model, Energy Environ. Sci. 13 (2020) 635–645.
[3] C. Zhu, J. Yuan, F. Cai, L. Meng, H. Zhang, H. Chen, J. Li, B. Qiu, H. Peng, S. Chen, Tuning the electron-deficient core of a non-fullerene acceptor to achieve over 17% efficiency in a single-junction organic solar cell, Energy Environ. Sci. 13 (2020) 2459–2466.
[4] Z. Luo, R. Ma, T. Liu, J. Yu, Y. Xiao, R. Sun, G. Xie, J. Yuan, Y. Chen, K. Chen, Fine-Tuning energy levels via asymmetric end groups enables polymer solar cells with efficiencies over 17%, Joule 4 (2020) 1236–1247.
[5] Z. Li, G. He, X. Wan, Y. Liu, J. Zhou, G. Long, Y. Zuo, M. Zhang, Y. Chen, Solution processable rhodanine-based small molecule organic photovoltaic cells with a power conversion efficiency of 6.1%, Advanced Energy Materials 2 (2012) 74–77.
[6] G. Feng, Y. Xu, J. Zhang, Z. Wang, Y. Zhou, Y. Li, Z. Wei, C. Li, W. Li, All-small-molecule organic solar cells based on an electron donor incorporating binary electron-deficient units, J. Mater. Chem. 4 (2016) 6056–6063.
[7] B. Walker, C. Kim, T.-Q. Nguyen, Small molecule solution-processed bulk heterojunction solar cells, Chem. Mater. 23 (2011) 470–482.
[8] J. Kong, S. Song, M. Yoo, G.Y. Lee, O. Kwon, J.K. Park, H. Back, G. Kim, S.H. Lee, H. Suh, Long-term stable polymer solar cells with significantly reduced burn-in loss, Nat. Commun. 5 (2014) 5688.
[9] J. Roncali, P. Leriche, P. Blanchard, Molecular materials for organic photovoltaics: small is beautiful, Adv. Mater. 26 (2014) 3821–3838.
[10] Y. Sun, G.C. Welch, W.L. Leong, C.J. Takacs, G.C. Bazan, A.J. Heeger, Solution-processed small-molecule solar cells with 6.7% efficiency, Nat. Mater. 11 (2012) 44–48.
[11] H. Bin, J. Yao, Y. Yang, I. Angunawela, C. Sun, L. Gao, L. Ye, B. Qiu, L. Xue, C. Zhu, High-efficiency all-small-molecule organic solar cells based on an organic molecule donor with alkylsilyl-thienyl conjugated side chains, Adv. Mater. 30 (2018), 1706361.
[12] H. Bin, Y. Yang, Z.-G. Zhang, L. Ye, M. Ghasemi, S. Chen, Y. Zhang, C. Zhang, C. Sun, L. Xue, 9.73% efficiency nonfullerene all organic small molecule solar cells with absorption-complementary donor and acceptor, J. Am. Chem. Soc. 139 (2017) 5085–5094.
[13] R.Z. Liang, M. Babics, V. Savikhin, W. Zhang, V.M. Le Corre, S. Lopatin, Z. Kan, Y. Firdaus, S. Liu, I. McCulloch, Carrier transport and recombination in efficient "all-small-molecule" solar cells with the nonfullerene acceptor IDTBR, Advanced Energy Materials 8 (2018) 1800264.
[14] L. Yang, S. Zhang, C. He, J. Zhang, Y. Yang, J. Zhu, Y. Cui, W. Zhao, H. Zhang, Y. Zhang, Modulating molecular orientation enables efficient nonfullerene small-molecule organic solar cells, Chem. Mater. 30 (2018) 2129–2134.
[15] R. Zhou, Z. Jiang, C. Yang, J. Yu, J. Feng, M.A. Adil, D. Deng, W. Zou, J. Zhang, K. Lu, All-small-molecule organic solar cells with over 14% efficiency by optimizing hierarchical morphologies, Nat. Commun. 10 (2019) 5393.
[16] S. Badgujar, C.E. Song, S. Oh, W.S. Shin, S.-J. Moon, J.-C. Lee, I.H. Jung, S.K. Lee, Highly efficient and thermally stable fullerene-free organic solar cells based on a small molecule donor and acceptor, J. Mater. Chem. 4 (2016) 16335–16340.
[17] X. Li, Y. Wang, Q. Zhu, X. Guo, W. Ma, X. Ou, M. Zhang, Y. Li, A small molecule donor containing a non-fused ring core for all-small-molecule organic solar cells with high efficiency over 11%, J. Mater. Chem. 7 (2019) 3682–3690.
[18] A. Mishra, P. Bäuerle, Small molecule organic semiconductors on the move: promises for future solar energy technology, Angew. Chem. Int. Ed. 51 (2012) 2020–2067.
[19] K. Sun, Z. Xiao, S. Lu, W. Zajaczkowski, W. Pisula, E. Hanssen, J.M. White, R. M. Williamson, J. Subbiah, J. Ouyang, A molecular nematic liquid crystalline material for high-performance organic photovoltaics, Nat. Commun. 6 (2015) 6013.
[20] J. Wan, X. Xu, G. Zhang, Y. Li, K. Feng, Q. Peng, Highly efficient halogen-free solvent processed small-molecule organic solar cells enabled by material design and device engineering, Energy Environ. Sci. 10 (2017) 1739–1745.
[21] Z.B. Henson, G.C. Welch, T. van der Poll, G.C. Bazan, Pyridalthiadiazole-based narrow band gap chromophores, J. Am. Chem. Soc. 134 (2012) 3766–3779.
[22] K. Gao, J. Miao, L. Xiao, W. Deng, Y. Kan, T. Liang, C. Wang, F. Huang, J. Peng, Y. Cao, Multi-length-scale morphologies driven by mixed additives in porphyrin-based organic photovoltaics, Adv. Mater. 28 (2016) 4727–4733.
[23] J. Gao, J. Ge, R. Peng, C. Liu, L. Cao, D. Zhang, B. Fanady, L. Hong, E. Zhou, Z. Ge, Over 14% efficiency nonfullerene all-small-molecule organic solar cells enabled by

improving the ordering of molecular donors via side-chain engineering, J. Mater. Chem. 8 (2020) 7405–7411.
[24] Q. Wei, W. Liu, M. Leclerc, J. Yuan, H. Chen, Y. Zou, A-DA′ DA non-fullerene acceptors for high-performance organic solar cells, Sci. China Chem. 13 (2020) 1142–1150.
[25] H. Tang, H. Chen, C. Yan, J. Huang, P.W. Fong, J. Lv, D. Hu, R. Singh, M. Kumar, Z. Xiao, Delicate morphology control triggers 14.7% efficiency all-small-molecule organic solar cells, Advanced Energy Materials 10 (2020), 2001076.
[26] L. Zhang, X. Liu, X. Sun, C. Duan, Z. Wang, X. Liu, S. Dong, F. Huang, Y. Cao, 4-Methylthio substitution on benzodithiophene-based conjugated polymers for high open-circuit voltage polymer solar cells, Synth. Met. 254 (2019) 122–127.
[27] W. Ni, M. Li, B. Kan, F. Liu, X. Wan, Q. Zhang, H. Zhang, T.P. Russell, Y. Chen, Fullerene-free small molecule organic solar cells with a high open circuit voltage of 1.15 V, Chem. Commun. 52 (2016) 465–468.
[28] R. Zhang, J. Wang, X. Liu, S. Pang, C. Duan, F. Huang, Y. Cao, High open-circuit voltage organic solar cells enabled by a difluorobenzoxadiazole-based conjugated polymer donor, Sci. China Chem. 62 (2019) 829–836.
[29] A. Tang, W. Song, B. Xiao, J. Guo, J. Min, Z. Ge, J. Zhang, Z. Wei, E. Zhou, Benzotriazole-based acceptor and donors, coupled with chlorination, achieve a high V OC of 1.24 V and an efficiency of 10.5% in fullerene-free organic solar cells, Chem. Mater. 31 (2019) 3941–3947.
[30] M. Babics, T. Duan, A.H. Balawi, R.-Z. Liang, F. Cruciani, I.-D. Carja, D. Gottlieb, I. McCulloch, K. Vandewal, F.d.r. Laquai, Negligible energy loss during charge generation in small-molecule/fullerene bulk-heterojunction solar cells leads to open-circuit voltage over 1.10 V, ACS Appl. Energy Mater. 2 (2019) 2717–2722.
[31] L. Huo, J. Hou, S. Zhang, H.Y. Chen, Y. Yang, A Polybenzo [1, 2-b: 4, 5-b′] dithiophene Derivative with Deep HOMO level and its application in high-performance polymer solar cells, Angew. Chem. 122 (2010) 1542–1545.
[32] L. Huo, S. Zhang, X. Guo, F. Xu, Y. Li, J. Hou, Replacing alkoxy groups with alkylthienyl groups: a feasible approach to improve the properties of photovoltaic polymers, Angew. Chem. Int. Ed. 50 (2011) 9697–9702.
[33] S.H. Liao, H.J. Jhuo, Y.S. Cheng, S.A. Chen, Fullerene derivative-doped zinc oxide nanofilm as the cathode of inverted polymer solar cells with low-bandgap polymer (PTB7-Th) for high performance, Adv. Mater. 25 (2013) 4766–4771.
[34] Y. Dong, X. Hu, C. Duan, P. Liu, S. Liu, L. Lan, D. Chen, L. Ying, S. Su, X. Gong, A series of new medium-bandgap conjugated polymers based on naphtho [1, 2-c: 5, 6-c] bis (2-octyl-[1, 2, 3] triazole) for high-performance polymer solar cells, Adv. Mater. 25 (2013) 3683–3688.
[35] G. Zhang, X. Xu, Z. Bi, W. Ma, D. Tang, Y. Li, Q. Peng, Fluorinated and alkylthiolated polymeric donors enable both efficient fullerene and nonfullerene polymer solar cells, Adv. Funct. Mater. 28 (2018), 1706404.
[36] S. Chen, Y. Liu, L. Zhang, P.C. Chow, Z. Wang, G. Zhang, W. Ma, H. Yan, A wide-bandgap donor polymer for highly efficient non-fullerene organic solar cells with a small voltage loss, J. Am. Chem. Soc. 139 (2017) 6298–6301.
[37] H. Yao, H. Zhang, L. Ye, W. Zhao, S. Zhang, J. Hou, Dialkylthio substitution: an effective method to modulate the molecular energy levels of 2D-BDT photovoltaic polymers, ACS Appl. Mater. Interfaces 8 (2016) 3575–3583.
[38] Z. Du, X. Bao, Y. Li, D. Liu, J. Wang, C. Yang, R. Wimmer, L.W. Städe, R. Yang, D. Yu, Balancing high open circuit voltage over 1.0 V and high short circuit current in benzodithiophene-based polymer solar cells with low energy loss: a synergistic effect of fluorination and alkylthiolation, Advanced Energy Materials 8 (2018), 1701471.
[39] X. Li, G. Huang, N. Zheng, Y. Li, X. Kang, S. Qiao, H. Jiang, W. Chen, R. Yang, High-efficiency polymer solar cells over 13.9% with a high VOC beyond 1.0 V by synergistic effect of fluorine and sulfur, Solar RRL 3 (2019), 1900005.
[40] C. Cui, W.-Y. Wong, Y. Li, Improvement of open-circuit voltage and photovoltaic properties of 2D-conjugated polymers by alkylthio substitution, Energy Environ. Sci. 7 (2014) 2276–2284.
[41] L. Ye, S. Zhang, W. Zhao, H. Yao, J. Hou, Highly efficient 2D-conjugated benzodithiophene-based photovoltaic polymer with linear alkylthio side chain, Chem. Mater. 26 (2014) 3603–3605.
[42] Y.-J. Cheng, J. Luo, S. Huang, X. Zhou, Z. Shi, T.-D. Kim, D.H. Bale, S. Takahashi, A. Yick, B.M. Polishak, Donor− acceptor thiolated polyenic chromophores exhibiting large optical nonlinearity and excellent photostability, Chem. Mater. 20 (2008) 5047–5054.
[43] L. Huo, Y. Zhou, Y. Li, Alkylthio-substituted polythiophene: absorption and photovoltaic properties, Macromol. Rapid Commun. 30 (2009) 925–931.
[44] C. Cui, Z. He, Y. Wu, X. Cheng, H. Wu, Y. Li, Y. Cao, W.-Y. Wong, High-performance polymer solar cells based on a 2D-conjugated polymer with an alkylthio side-chain, Energy Environ. Sci. 9 (2016) 885–891.
[45] C. Cui, W.Y. Wong, Effects of alkylthio and alkoxy side chains in polymer donor materials for organic solar cells, Macromol. Rapid Commun. 37 (2016) 287–302.
[46] H. Zhang, H. Yao, J. Hou, J. Zhu, J. Zhang, W. Li, R. Yu, B. Gao, S. Zhang, J. Hou, Over 14% efficiency in organic solar cells enabled by chlorinated nonfullerene small-molecule acceptors, Adv. Mater. 30 (2018), 1800613.
[47] W. Zhao, S. Li, H. Yao, S. Zhang, Y. Zhang, B. Yang, J. Hou, Molecular optimization enables over 13% efficiency in organic solar cells, J. Am. Chem. Soc. 139 (2017) 7148–7151.
[48] B. Kan, J. Zhang, F. Liu, X. Wan, C. Li, X. Ke, Y. Wang, H. Feng, Y. Zhang, G. Long, Fine-tuning the energy levels of a nonfullerene small-molecule acceptor to achieve a high short-circuit current and a power conversion efficiency over 12% in organic solar cells, Adv. Mater. 30 (2018), 1704904.
[49] H. Feng, Y.Q.Q. Yi, X. Ke, J. Yan, Y. Zhang, X. Wan, C. Li, N. Zheng, Z. Xie, Y. Chen, New anthracene-fused nonfullerene acceptors for high-efficiency organic solar cells: energy level modulations enabling match of donor and acceptor, Advanced Energy Materials 9 (2019), 1803541.
[50] S. Li, L. Ye, W. Zhao, H. Yan, B. Yang, D. Liu, W. Li, H. Ade, J. Hou, A wide band gap polymer with a deep highest occupied molecular orbital level enables 14.2% efficiency in polymer solar cells, J. Am. Chem. Soc. 140 (2018) 7159–7167.
[51] N. Bauer, Q. Zhang, J.J. Rech, S. Dai, Z. Peng, H. Ade, J. Wang, X. Zhan, W. You, The impact of fluorination on both donor polymer and non-fullerene acceptor: the more fluorine, the merrier, Nano Research 12 (2019) 2400–2405.
[52] D. Deng, Y. Zhang, J. Zhang, Z. Wang, L. Zhu, J. Fang, B. Xia, Z. Wang, K. Lu, W. Ma, Fluorination-enabled optimal morphology leads to over 11% efficiency for inverted small-molecule organic solar cells, Nat. Commun. 7 (2016) 13740.
[53] A.K. Agrawal, S.A. Jenekhe, New conjugated polyanthrazolines containing thiophene moieties in the main chain, Macromolecules 24 (1991) 6806–6808.
[54] A.K. Agrawal, S.A. Jenekhe, Synthesis and processing of heterocyclic polymers as electronic, optoelectronic, and nonlinear optical materials. 2. New series of conjugated rigid-rod polyquinolines and polyanthrazolines, Macromolecules 26 (1993) 895–905.
[55] A.K. Agrawal, S.A. Jenekhe, Synthesis and processing of heterocyclic polymers as electronic, optoelectronic, and nonlinear optical materials. 3. New conjugated polyquinolines with electron-donor or-acceptor side groups, Chem. Mater. 5 (1993) 633–640.
[56] C.-Y. Kim, J.-G. Park, M.-J. Lee, S.-K. Kwon, J.-H. Kim, S.-C. Shin, Y.-H. Kim, Poly (1, 4-bis ((E)-2-(3-dodecylthiophen-2-yl) vinyl) benzene) for solution processable organic thin film transistor, Bull. Kor. Chem. Soc. 33 (2012) 1659–1663.
[57] Z. Wang, X. Zhu, J. Zhang, K. Lu, J. Fang, Y. Zhang, Z. Wang, L. Zhu, W. Ma, Z. Shuai, From alloy-like to cascade blended structure: designing high-performance all-small-molecule ternary solar cells, J. Am. Chem. Soc. 140 (2018) 1549–1556.
[58] L. Yang, S. Zhang, C. He, J. Zhang, H. Yao, Y. Yang, Y. Zhang, W. Zhao, J. Hou, New wide band gap donor for efficient fullerene-free all-small-molecule organic solar cells, J. Am. Chem. Soc. 139 (2017) 1958–1966.
[59] B. Kan, Q. Zhang, M. Li, X. Wan, W. Ni, G. Long, Y. Wang, X. Yang, H. Feng, Y. Chen, Solution-processed organic solar cells based on dialkylthiol-substituted benzodithiophene unit with efficiency near 10%, J. Am. Chem. Soc. 136 (2014) 15529–15532.
[60] J.-L. Wang, Z. Wu, J.-S. Miao, K.-K. Liu, Z.-F. Chang, R.-B. Zhang, H.-B. Wu, Y. Cao, Solution-processed diketopyrrolopyrrole-containing small-molecule organic solar cells with 7.0% efficiency: in-depth investigation on the effects of structure modification and solvent vapor annealing, Chem. Mater. 27 (2015) 4338–4348.
[61] Q. Wang, B. Xia, J. Xu, X. Niu, J. Cai, Q. Shen, W. Wang, W. Huang, Q. Fan, Biocompatible small organic molecule phototheranostics for NIR-II fluorescence/photoacoustic imaging and simultaneous photodynamic/photothermal combination therapy, Materials Chemistry Frontiers 3 (2019) 650–655.
[62] Z. Wang, X. Xu, Z. Li, K. Feng, K. Li, Y. Li, Q. Peng, Solution-processed organic solar cells with 9.8% efficiency based on a new small molecule containing a 2D fluorinated benzodithiophene central unit, Advanced Electronic Materials 2 (2016), 1600061.
[63] W. Ni, M. Li, X. Wan, H. Feng, B. Kan, Y. Zuo, Y. Chen, A high-performance photovoltaic small molecule developed by modifying the chemical structure and optimizing the morphology of the active layer, RSC Adv. 4 (2014) 31977–31980.
[64] K.-W. Chen, L.-Y. Lin, Y.-H. Li, Y.-Z. Li, T.P. Nguyen, S. Biring, S.-W. Liu, K.-T. Wong, Fluorination effects of ADA-type small molecules on physical property and the performance of organic solar cell, Org. Electron. 52 (2018) 342–349.
[65] J.W. Jo, J.W. Jung, E.H. Jung, H. Ahn, T.J. Shin, W.H. Jo, Fluorination on both D and A units in D–A type conjugated copolymers based on difluorobithiophene and benzothiadiazole for highly efficient polymer solar cells, Energy Environ. Sci. 8 (2015) 2427–2434.
[66] G. Ren, C.W. Schlenker, E. Ahmed, S. Subramaniyan, S. Olthof, A. Kahn, D. S. Ginger, S.A. Jenekhe, Photoinduced hole transfer becomes suppressed with diminished driving force in polymer-fullerene solar cells while electron transfer remains active, Adv. Funct. Mater. 23 (2013) 1238–1249.
[67] H. Yao, F. Bai, H. Hu, L. Arunagiri, J. Zhang, Y. Chen, H. Yu, S. Chen, T. Liu, J.Y. L. Lai, Efficient all-polymer solar cells based on a new polymer acceptor achieving 10.3% power conversion efficiency, ACS Energy Letters 4 (2019) 417–422.
[68] E. Lee, W. Shin, O. Bae, F.S. Kim, Y.-J. Hwang, Synthesis and Characterization of a highly crystalline benzotriazole-selenophene copolymer semiconductor, Polymer 184 (2019), 121856.
[69] Y.-J. Hwang, N.M. Murari, S.A. Jenekhe, New n-type polymer semiconductors based on naphthalene diimide and selenophene derivatives for organic field-effect transistors, Polym. Chem. 4 (2013) 3187–3195.
[70] B.A. Courtright, S.A. Jenekhe, Polyethylenimine interfacial layers in inverted organic photovoltaic devices: effects of ethoxylation and molecular weight on efficiency and temporal stability, ACS Appl. Mater. Interfaces 7 (2015) 26167–26175.
[71] X. He, L. Yin, Y. Li, Design of organic small molecules for photovoltaic application with high open-circuit voltage (V oc), J. Mater. Chem. C 7 (2019) 2487–2521.
[72] M.G. Walter, E.L. Warren, J.R. McKone, S.W. Boettcher, Q. Mi, E.A. Santori, N. S. Lewis, Solar water splitting cells, Chem. Rev. 110 (2010) 6446–6473.
[73] Y. Gao, V.M. Le Corre, A. Gaïtis, M. Neophytou, M.A. Hamid, K. Takanabe, P. M. Beaujuge, Homo-Tandem polymer solar cells with VOC > 1.8 V for efficient PV-driven water splitting, Adv. Mater. 28 (2016) 3366–3373.